

Disentangling the Roles of Dissolved Oxygen, Common Salts, and pH on the Spontaneous Hydrogen Peroxide Production in Water: No O₂, No H₂O₂

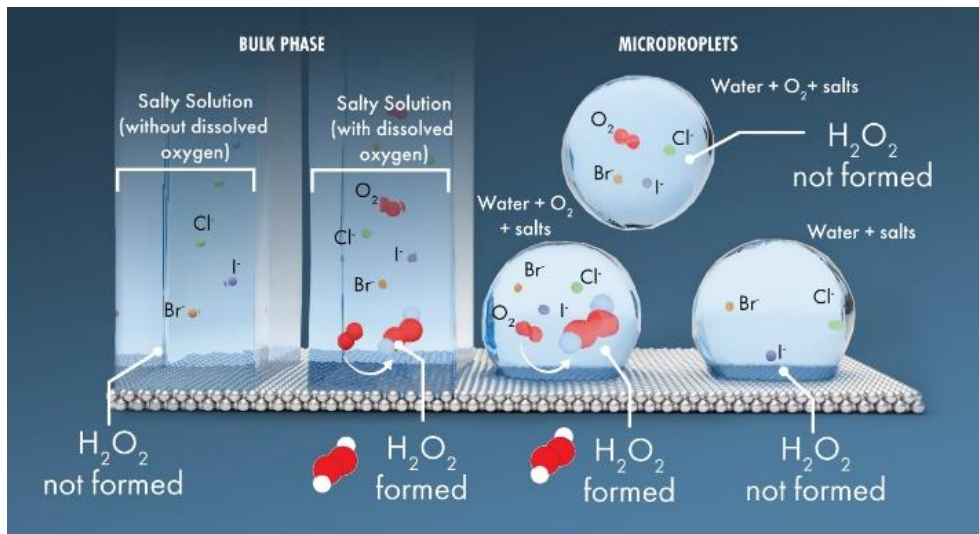
Muzzamil Ahmad Eatoo^{1,2,*} & Himanshu Mishra^{1,2,*}

¹ Environmental Science and Engineering (EnSE) Program, Biological and Environmental Science and Engineering (BESE) Division, King Abdullah University of Science and Technology (KAUST), Thuwal, 23955-6900, Kingdom of Saudi Arabia

² Interfacial Lab (iLab), King Abdullah University of Science and Technology (KAUST), Thuwal 23955-6900, Saudi Arabia

*Correspondence: muzzamil.eatoo@kaust.edu.sa and himanshu.mishra@kaust.edu.sa

TOC Image



Abstract:

Despite the mounting evidence proving that the air–water interface or the microdroplet geometry has nothing to do with the spontaneous formation of hydrogen peroxide (H_2O_2), the myth persists. Three recent studies by George & co-workers give credence to the myth by showing connections between the spontaneous formation of hydroxyl (HO^\bullet) radicals and hydrogen peroxide (H_2O_2) in sprayed microdroplets with the solution pH, dissolved salts, nebulizing gas, and the gaseous environment. They report that among halides (Cl^- , Br^- , and I^-), Br^- dominates the H_2O_2 formation because of its ability to donate electrons. Also, they conclude that the H_2O_2 production at the air–water interface scales with water’s alkalinity. In response, we apply a broad set of techniques, spanning ^1H -NMR, potentiodynamic polarization, electron microscopy, and hydrogen peroxide assay kit (HPAK) fluorometry, to reexamine these claims. Our experiments reveal that regardless of the halide present in water, the air–water interface or the microdroplet geometry does not drive the H_2O_2 formation. In fact, it is the reduction of O_2 at the solid–water interface, that produces H_2O_2 , i.e., in the absence of O_2 , no H_2O_2 is formed regardless of the halide. We explain the relative dependence of H_2O_2 concentrations on the halides based on their propensity to drive pitting corrosion ($\text{Cl}^- > \text{Br}^- > \text{I}^-$). As the pits appear in the passivating layer, exposing the metal, H_2O_2 is consumed in further oxidation. Next, we disprove the claim of alkalinity-driven H_2O_2 formation by demonstrating that aluminum and titanium surfaces more H_2O_2 in acidic and alkaline conditions, respectively. Taken together, these findings refute the conclusions of George & co-workers and others regarding spontaneous H_2O_2 generation at the air-water interface. The following mnemonic captures our conclusion: no O_2 , no H_2O_2 .

Introduction:

The spontaneous formation of H_2O_2 in water microdroplets, without a catalyst or external energy, has sparked one of the most prominent debates in the chemical science community. Zare & co-workers have claimed that water microdroplets (<20 μm diameter) formed via pneumatic spraying or condensation spontaneously generate hydrogen peroxide (H_2O_2); albeit, the reported quantities have varied from 180–0.3 μM in the last 6 years¹⁻⁵. They have maintained that ultrahigh electric field fluctuations at the air–water interface are responsible for this chemical transformation, basing on the studies led by Mundy⁶, Amotz⁷, Head-Gordon⁸, and Min⁹. Contrary to the mechanism suggested by Head-Gordon & co-workers, Colussi^{10, 11} has put forth a thermochemistry-based argument that entails dehydration of ions at the air–water interface driving the H_2O_2 formation, and Cooks¹² has been suggested that the water radical cation is responsible for this chemistry. Is this a hitherto unrealized anomalous property of water?

Our group has challenged these claims and conclusions by demonstrating that the microdroplet geometry or the air–water interface, and, therefore, the ultrahigh instantaneous electric fields therein, do not generate H_2O_2 .¹³⁻¹⁶ Potential artifacts arising from the use of ultrasonication while creating microdroplets¹⁶ and ambient contamination¹⁵ have been pointed out. As well, we have demonstrated that small quantities of H_2O_2 (~1 μM) may be formed spontaneously at water–solid interfaces, implicated in these experiments, due to the reduction of dissolved oxygen gas (O_2)¹⁴. As a corollary, we have demonstrated that if O_2 is eliminated from the water, then H_2O_2 is not formed in the sprays or at the solid–water interface down to a 50 nM detection limit¹⁴. Recently, Koppenol & co-workers¹⁷, Ruiz-Lopez and co-workers¹⁸, Hassanali & co-workers¹⁹, Williams & co-workers^{20, 21}, and Rodríguez-López & co-workers²², have corroborated our findings through complementary approaches based on thermodynamics, quantum chemistry, mass spectrometry, electrochemistry, and electron spin resonance. For additional resources, see refs.^{5, 23-28}.

Despite the evidence, the myth of H_2O_2 generation in water microdroplets persists. A recent experimental report from George & coworkers gives credence to the electric field argument²⁹. They also investigated the effects of sodium salts (NaX | X: Cl^- , Br^- , or I^-) on the H_2O_2 production in sprayed microdroplets³⁰. They conclude that H_2O_2 forms specifically at the air–water interface under the effect of ultrahigh electric fields via the following two mechanisms:(i)

OH^- ions undergo charge separation to form HO^\bullet and e^- , and HO^\bullet radicals form H_2O_2 , or (ii) Br^- ions undergo charge separation to form Br^\bullet and e^- ; next, dissolved oxygen (O_2) reacts with e^- and H^+ to form HO_2^\bullet , which reacts with H^\bullet (produced from the reaction between $\text{H}^+ + \text{e}^-$) to form H_2O_2 . Their experiments reveal that at concentrations below 1mM, Cl^- ions generate the highest H_2O_2 concentration in the sprays, while at concentrations above 1mM Br^- ions dominate the generation of H_2O_2 . However, they conclude that “*only Br^- contributes to the interfacial H_2O_2 formation, promoting the production by acting as an electron donor*”.³⁰ Lastly, they reported that in the presence of NaCl or Na_2SO_4 , the H_2O_2 production increases by approximately 40% under alkaline conditions (pH 9) compared to acidic conditions (pH 4)³¹. They attribute all these observations to be arising at the air–water interface, where OH^- and/or Br^- ions drive the H_2O_2 formation.

We consider that there are several actors in the H_2O_2 story – water, its intrinsic ions, O_2 , halides, the air–water interface, and various solid–water interfaces – which complicate the interpretation of the results. The last actor represents the incorrigible solid–water interfaces that come into play at various stages of the experiments, viz., during sample preparation (e.g., beakers and glass vials), spraying (e.g., tubing comprised of insulators or metals or alloys) or substrate for condensation, analyte collection (e.g., glassware), transferring (e.g., pipettes), and analytical measurement (e.g., vials, cuvettes, or NMR tubes). So, even if one is forming sprays, it must be checked whether the H_2O_2 formation takes place prior to spraying or after spraying. Here, we re-examine the claims of George & co-workers²⁹⁻³¹ by probing H_2O_2 formation due to O_2 reduction and surface oxidation of Al and Ti as representative materials as a function of halides and the water pH. The following interrelated questions are addressed:

1. Is it possible to spontaneously generate H_2O_2 at the air–water interface or the solid–water interface in the absence of O_2 ? In this scenario, do halides play any role?
2. Conversely, what is the influence of halides on the H_2O_2 formation in the presence of O_2 , such as water in equilibrium with the air? In this scenario, where does the H_2O_2 formation take place: the air–water interface or the solid–water interface?
3. In the experiments of George & co-workers³⁰, why did microdroplets containing Br^- at > 1 mM concentration generate higher H_2O_2 than those containing Cl^- or I^- ? Is it due to Br^- ions’ ability to undergo “charge separation” to form $\text{Br}^\bullet + \text{e}^-$ at the air–water interface? If not, could this be explained based on solid surface oxidation?

4. At concentrations < 1 mM, why did the H_2O_2 formation in salty microdroplets follow the order $\text{Cl}^- > \text{Br}^-$ (See Fig.2 in Ref.³⁰)? What is the role of solid–water interfaces?
5. Does H_2O_2 formation always increase with the water pH, as claimed by George & co-workers³²? Could you present a counter case?

While our experiments reproduce the observations of George & co-workers, we contest their conclusions and provide alternative explanations. Crucially, the H_2O_2 generation takes place at the water–solid interfaces due to the reduction of O_2 , i.e., the air-water interface or the microdroplet geometry has no bearing on this chemical transformation.

Results

Effects of halides on the spontaneous formation of H_2O_2 in microdroplets

Firstly, H_2O_2 formation was quantified in pneumatic sprays formed with 10 mM salt solutions of Na^+X^- , where X: Cl, Br, or I, and compared with that in the sprays formed with bulk water (Figure 1a and Methods). Prior to spraying, the bulk solutions were divided into two batches: (i) those containing O_2 as per the Henry's law (~ 4 mg/l at normal temperature and pressure)³³, and (ii) solutions with negligible O_2 , achieved by boiling, followed by $\text{N}_2(\text{g})$ bubbling for 45 minutes and keeping them inside an N_2 -purged container (Methods). Note: the latter batch had an O_2 concentration < 0.01 mg/l, as measured via an O_2 sensor (WTW Multi 3320). In a clean glovebox filled with N_2 gas, microdroplets were generated by shearing streams of abovementioned bulk solutions – flowing at the rate of $25\mu\text{L}/\text{min}$ through a 0.10 mm-wide silica capillary – through pressurized $\text{N}_2(\text{g})$ gas (100 psi) flowing through an outer concentric tube of 0.43 mm in diameter (Figures 1a-b & S1). Inside the N_2 environment, sprayed microdroplets were collected in clean glassware and transferred for analytical measurement. The quantification of H_2O_2 was done by two methods, namely (1) ^1H -NMR using a Bruker 950 MHz Avance Neo NMR spectrometer equipped with a 5 mm Z-axis gradient TCI cryoprobe at the temperature of 275 K (50,000 scans with a 50-ms acquisition time and a 1 ms recycle delay between scans), following the protocol of Bax and co-workers³⁴, and (2) Hydrogen Peroxide Assay Kit (HPAK) for H_2O_2 quantification (Methods). The limits of detection were ≥ 50 nM and ≥ 250 nM for ^1H -NMR and HPAK, respectively. While NMR guaranteed an unambiguous fingerprinting of H_2O_2 , it took ~ 2 hrs for scanning time per sample; on the other hand, HPAK offered speed and ease but may be vulnerable to false positives due to chemical interference.

To get the best from either scenario, we cross-validated all the H_2O_2 measurements with both techniques and found them to be consistent.

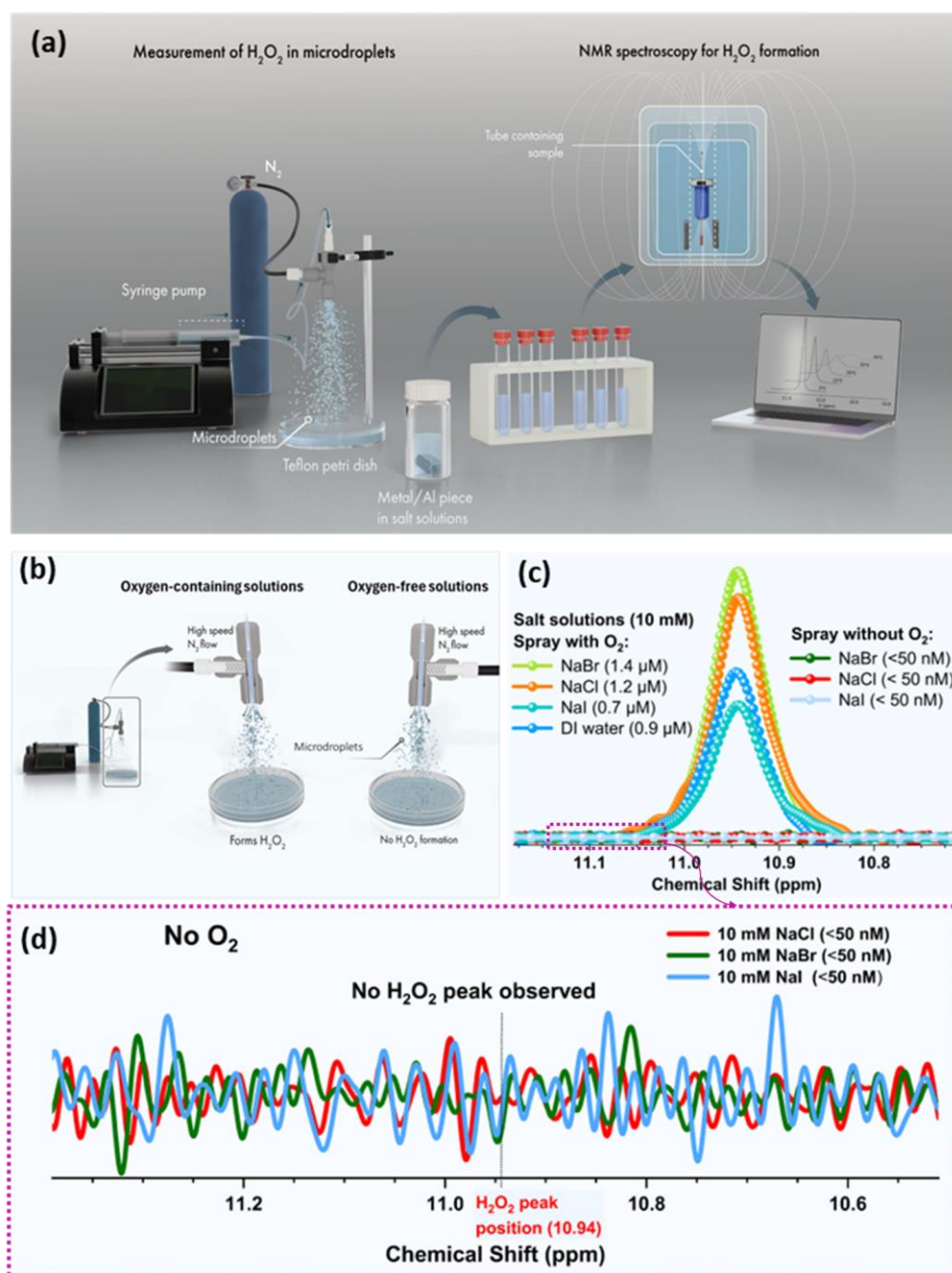


Figure 1. (a) Illustration of the experimental setup showing the complete path of H_2O_2 investigations in microdroplets by forming microdroplets using high-pressure dry N_2 gas and then analyzing the samples using ^1H -NMR spectroscopy. (b) Illustration of the spray setup to nebulize aqueous streams with and without O_2 using high-pressure N_2 gas to form microdroplets. The roles of dissolved oxygen (O_2) and 10 mM salt (Na^+X^- , where X: Cl, Br, or I) concentration on the H_2O_2 formation were probed via ^1H -NMR. (c) Results reveal that in the absence of O_2 , no H_2O_2 was formed (detection limit ≥ 50 nM) regardless of the salt. In the presence of O_2 (i.e., solutions saturated with the air), the formation of H_2O_2 varied with the salt type. Note: these samples were also analyzed by HPAK, and the results are presented in Figure S2. (d) ^1H -NMR results of oxygen-free N_2 -sprayed salty microdroplets confirming no H_2O_2 formation.

The experimental results revealed that for the solutions devoid of O₂, sprayed microdroplets did not contain any detectable H₂O₂, regardless of the salt (Note: the limit of detection was ≥ 50 nM) (Figure 1c-d). **This is smoking gun evidence that the air–water interface or the microdroplet geometry or the ultrahigh instantaneous electric fields do not form H₂O₂**, contradicting several proposed mechanisms^{8, 10-12}. Notably, in the absence of O₂, solid–water interfaces also do not form H₂O₂. No wonder, George & coworkers observed a 91% decline in the formation of H₂O₂ when they formed microdroplets in a N₂ gas environment³⁰. We surmise that the remaining 9% signal was due to the O₂ dissolved in their solutions (~ 4 mg/l at normal temperature and pressure)³³.

When O₂ was present in the water, then the ensuing microdroplets contained H₂O₂, and the concentration varied with the halides as: Br⁻ > Cl⁻ > DI water > I⁻ (Figure 1-c & S2). While the trend is aligned with the observation of George & co-workers, we doubted that it was due to their charge separation hypothesis³⁰. Therefore, we broadened our study to investigate O₂ reduction and solid surface oxidation in the presence of halides.

Effects of halides on the spontaneous formation of H₂O₂ at solid–water interfaces

We chose a common aluminium alloy (AA5083) as the representative material to probe the effects of halides on the spontaneous formation of H₂O₂ at solid–liquid interfaces. Freshly polished aluminium specimens of known surface area (~ 2.3 cm²) were immersed in ~ 2 ml volume of salt solutions (Figure 2a), equilibrated with air inside sealed glass vials, and the H₂O₂ concentrations were measured after 1 hr (with HPAK and cross-checked by ¹H-NMR). For all the halides, H₂O₂ was formed in bulk water in contact with Al plate (Figure 2b). These results, as well as our prior work with a number of metal surfaces such as Mg, Al, and Si, in the presence or absence of O₂, reveal that H₂O₂ is formed during the reduction of O₂ at the solid–liquid interfaces¹⁴. Figure 2c sheds light on the mechanism –the solid surface oxidizes to soluble products such as metal ions (Mⁿ⁺) and insoluble products such as oxides (MO_x) and hydroxides (M(OH)_y). The insoluble oxidation products form a protective passive layer on the material surface and slow down the oxidation process.

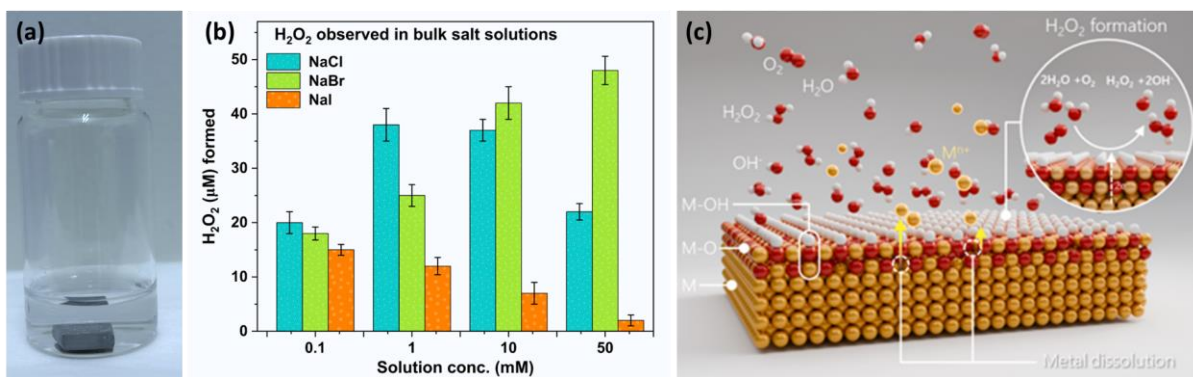


Figure 2 Effects of 0–50 mM Na^+X^- salts, where X: Cl, Br, or I, on the spontaneous H_2O_2 formation at the solid–liquid interface in the presence of O_2 . (a) Freshly polished aluminium specimens were immersed in salt solutions that were equilibrated with air. (b) After 1hr of immersion, the H_2O_2 formation at the Al–solution interface for halide concentrations ≤ 1 mM, followed the trend: $\text{Cl}^- > \text{Br}^- > \text{I}^-$, and (ii) For halide concentrations ≥ 10 mM, the H_2O_2 formation follows the trend: $\text{Br}^- > \text{Cl}^- > \text{I}^-$. (c) Illustration showing the oxidation of the metal surface at the solid–water interface and the reduction of O_2 to produce H_2O_2 . N.B.: Al–water interfacial area of 2.3 cm^2 in 10 mM bulk solutions (2 ml).

Curiously, two trends appeared depending on the halides' concentrations (Figure 2b): (i) for salt concentrations ≤ 1 mM, the H_2O_2 formation followed the order: $\text{Cl}^- > \text{Br}^- > \text{I}^-$, and (ii) for salt concentrations ≥ 10 mM, the H_2O_2 formation followed the order: $\text{Br}^- > \text{Cl}^- > \text{I}^-$. Clearly, the mechanism based on Br^- ions' speciation to the air–water interface, followed by charge separation, fails to explain this observation. Thus, we wondered if the halides could influence the oxidation rates of solid surfaces and be implicated in H_2O_2 formation.

Quantifying Oxidation Rates of Solid Surfaces in the Presence of Salts

To answer the question raised above, we probed the effects of halides on O_2 reduction at the solid–water interface. Aluminum alloy (AA5083) was chosen as the representative material because its oxidation rate can be accurately captured via electrochemical measurements. To gain insights into the surface oxidation (or corrosion), we utilized a potentiodynamic polarization technique (Methods). Typical experiments entailed a three-electrode electrochemical cell with a freshly polished substrate ($\sim 1 \text{ cm}^2$) as the working electrode, a platinum plate ($\sim 1 \text{ cm}^2$) as a counter-electrode, and a reference saturated calomel electrode (Methods). To quantify the oxidation rate, first, the open circuit potential (OCP) was measured and then, the potentiodynamic polarization test was commenced at -500 mV below the OCP, scanning a range up to $\text{OCP} + 1000 \text{ mV}$ at the rate of $+0.5 \text{ mV s}^{-1}$. Current densities

from these measurements yielded the oxidation rate (or the corrosion rate) due to O_2 and the the specific roles of the salts. Figure 3a&b. We found that the surface oxidation rates increased with the salt concentration and always varied with the halides as: $Cl^- > Br^- > I^-$.

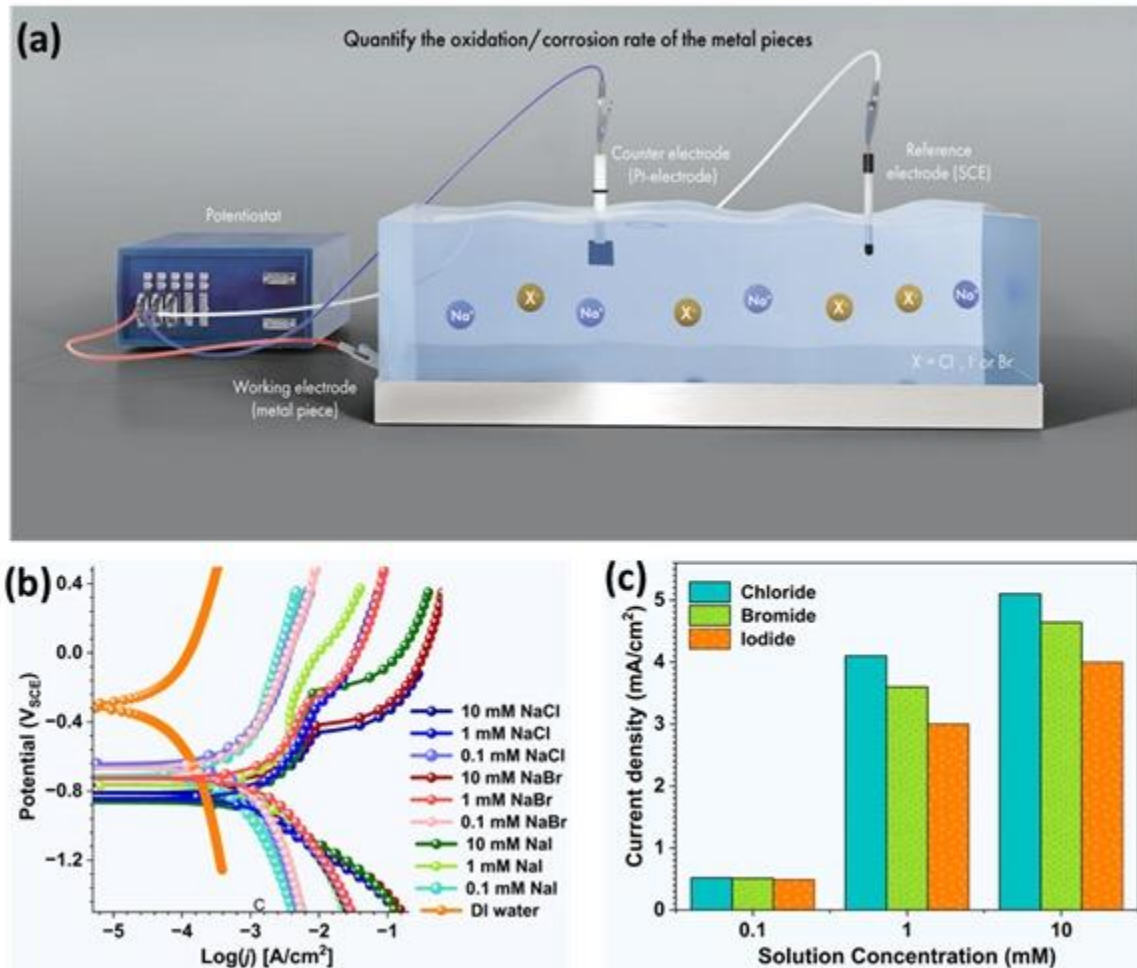


Figure 3. The effect of salts on the oxidation rate of solid/Al at SWI. (a) Illustration showing the electrochemical testing setup. It shows a three-electrode cell that consists of a metal surface under investigation acting as the working electrode, a platinum electrode as the counter electrode, and a saturated calomel electrode as the reference electrode. (b) Potentiodynamic polarization curves showing oxidation/corrosion behaviors of solid/Al surface in different halide anion solutions. (c) Corrosion current densities of the Al (AA5083) surface in different salt solutions calculated from polarization curves. It shows that the oxidation rate of Al in different halide solutions follows the trend $Cl^- > Br^- > I^-$.

Several consistencies and inconsistencies arise as we compare the trends in measured H_2O_2 concentrations in sprays (Figure 2b) and the corrosion at the solid–water interface (Figures 3b-c). Firstly, the observed oxidation rates of the metal surface (Figure 3c) follow the same trends as those of the H_2O_2 formation at the metal–water interface for salt concentrations ≤ 1 mM, i.e., $Cl^- > Br^- > I^-$ (Figure 2b). However, for salt concentrations ≥ 10 mM, the H_2O_2

formation follows a different order: $\text{Br}^- > \text{Cl}^- > \text{I}^-$ (Figure 2b). Next, for I^- , whereas the oxidation rates keep on increasing with the concentration, the measured H_2O_2 concentrations follow the opposite trend. How do we reconcile these findings?

The Curious Case of Cl^- and Br^- vis-à-vis Surface Oxidation

To understand why the H_2O_2 formation at the solid–water interface decreases with the Cl^- concentration ≥ 10 mM, one has to dive into the fundamentals of pitting corrosion³⁵. It refers to the formation of a pit across the passive oxide layer, exposing the fresh metal surface and restarting corrosion. Extensive scientific literature reveals that the halide ions' ability to cause pitting follows this trend: $\text{F}^- > \text{Cl}^- \gg \text{Br}^- > \text{I}^-$.^{36, 37} Pitting depends on the material characteristics and the halide concentration. For instance, for the aluminum alloy chosen in this work, pitting becomes aggressive at ≥ 10 mM (Figure S4a). So, while pitting is insignificant at 1 mM concentration, it becomes severe at 10 mM, exposing a fresh metal surface. As the fresh metal surface comes into contact with H_2O_2 , oxidation follows. As shown in Figure S4-a, the onset of pitting is marked by a sharp rise in the current density. Interestingly, H_2O_2 that was formed initially as the byproduct of O_2 reduction at the solid–water interface is now consumed during pitting. As pitting by Cl^- ions continues, and this process repeats, the H_2O_2 concentration keeps decreasing. This reconciles the concentration-dependent trends in the measured H_2O_2 concentration above and the measured current densities (Figures 2b & 3c), and calls into question the explanation put forth by George & co-workers³⁰.

The Curious Case of I^- vis-à-vis Surface Oxidation

The formation of H_2O_2 at the solid–water interface decreases with increasing NaI concentration, as presented in Fig. 2b and also noted by George & co-workers³⁰. This can be explained based on the reaction of H_2O_2 with iodide ions, leading to the formation of triiodide (I_3^-). See Figure S3, where the evidence for the formation of I_3^- is presented.

Reconciling H_2O_2 formation and O_2 Reduction at the Solid–Water Interfaces

Based on the experimental results (Figs. 2, 3, S4, and S7), it is clear that the peculiar properties of halides vis-à-vis pitting and reactivity with H_2O_2 lead to their consumption over time. To prove that the H_2O_2 formation is directly proportional to the oxidation of solid surfaces, we devised a new experiment. We exploited the fast reactivity of the hydrogen

peroxide assay kit (HPAK) reaction mixture with H_2O_2 , leading to a fluorescent product, to preempt its consumption by pitting or Γ . Metal (Al) specimens were immersed in a 1:1 volumetric mixture comprised of HPAK kit and 10 mM salt solutions and the fluorescence was measured. The results reveal that the H_2O_2 formation at the solid–water interface followed the same order as that of the oxidation rate of the solid surface, i.e., $\text{Cl}^- > \text{Br}^- > \text{I}^-$ (Figure 4).

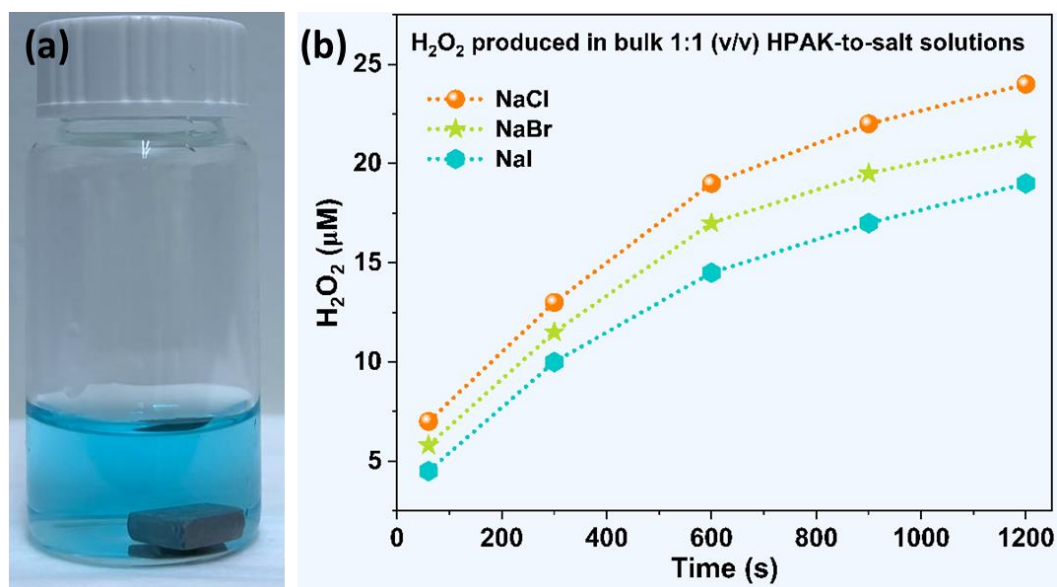


Figure 4 Time-dependent measurement of H_2O_2 formation at the solid–water interface in solutions obtained by mixing 10 mM Na^+X^- solutions, where X: Cl, Br, or I, with HPAK reaction mixture (1:1 v/v). See details of the measurements in the Methods section.

In summary, we noted that H_2O_2 formation is directly related to the oxidation of the solid surface: no O_2 , no H_2O_2 . The H_2O_2 formation is highest in NaCl solution, followed by NaBr, and least in NaI solution, having the same salt concentrations, their tendency to accelerate the corrosion or oxidation of the solid/Al surface follows the same order. Our findings explain the dataset of George & coworkers³⁰ in great detail and refute their mechanism that suggests that Br^- drives the H_2O_2 formation at the air–water interface due to charge separation.

Effect of water pH on the formation of H_2O_2 at the solid–water interfaces

Lastly, we examined the claims of George & co-workers³¹ for the pH-dependence of H_2O_2 formation, i.e., the higher the alkalinity, the higher the H_2O_2 formation. We apply our framework of finding the equivalence between O_2 reduction and solid surface oxidation vis-à-

vis H₂O₂ formation. To do this, we chose aluminum and titanium as representative materials due to their contrasting pH-dependent oxidation behavior, i.e., Ti is known to passivate more (less oxidation) in acidic solutions, while Al passivates more in alkaline solutions. This way, we could disentangle the contributions of the solution alkalinity versus the surface oxidation towards H₂O₂ formation.

Specimens of the Al alloy (AA5083) with a surface area of 2.3 cm² were immersed in the following aqueous solutions (2 ml volume) equilibrated with air (i.e., containing O₂) for 1 hour: water (pH 5.6), pH 2 water (adjusted with HCl), and pH 10 (adjusted with NaOH). HPAK measurements (and cross-validation by 1H-NMR) revealed that for the Al–water interface, the H₂O₂ formation followed the following trend: pH 2 (~47 μM) > pH 10 (~14 μM) > water (~4.5 μM) (Figure 5a). In contrast, the Ti–water interface exhibited the following trend for the H₂O₂ formation: pH 10 (~0.88 μM) > pH 2 (~0.42 μM) > water (~0.22 μM) in one hour (Figure 5b). These results demonstrate that the previously proposed mechanisms for the pH as a driver for enhancing OH⁻ ions at the air–water interface, leading to the H₂O₂ formation, are wrong^{32 31}. Instead, it is the nature of the solid surface that gets oxidized that governs the pH-dependence of the H₂O₂ formation. To elucidate the last point further, we utilized the electrochemical potentiodynamic polarization technique to quantify the oxidation behaviors of Al and Ti specimens immersed in solutions of acidic/alkaline/neutral pH for 1 hour. The experimental results revealed that the oxidation rates exhibited the same trends as the H₂O₂ formation vis-à-vis the solution pH (Figures 5c–d). Specifically, the corrosion/oxidation rate (*i*_{corr}) of Al followed the order: *i*_{corr} acidic solution (~118.5 mA/cm²) > *i*_{corr} alkaline solution (~2.8 mA/cm²) > *i*_{corr} DI water (~79.4 μA/cm²) (Figure 5c). For Ti, the corrosion rate (*i*_{corr}) followed the order *i*_{corr} alkaline solution (~2.8 mA/cm²) > *i*_{corr} acidic solution (~0.45 mA/cm²) > *i*_{corr} DI water (~0.063 mA/cm²) (Figure 5d).

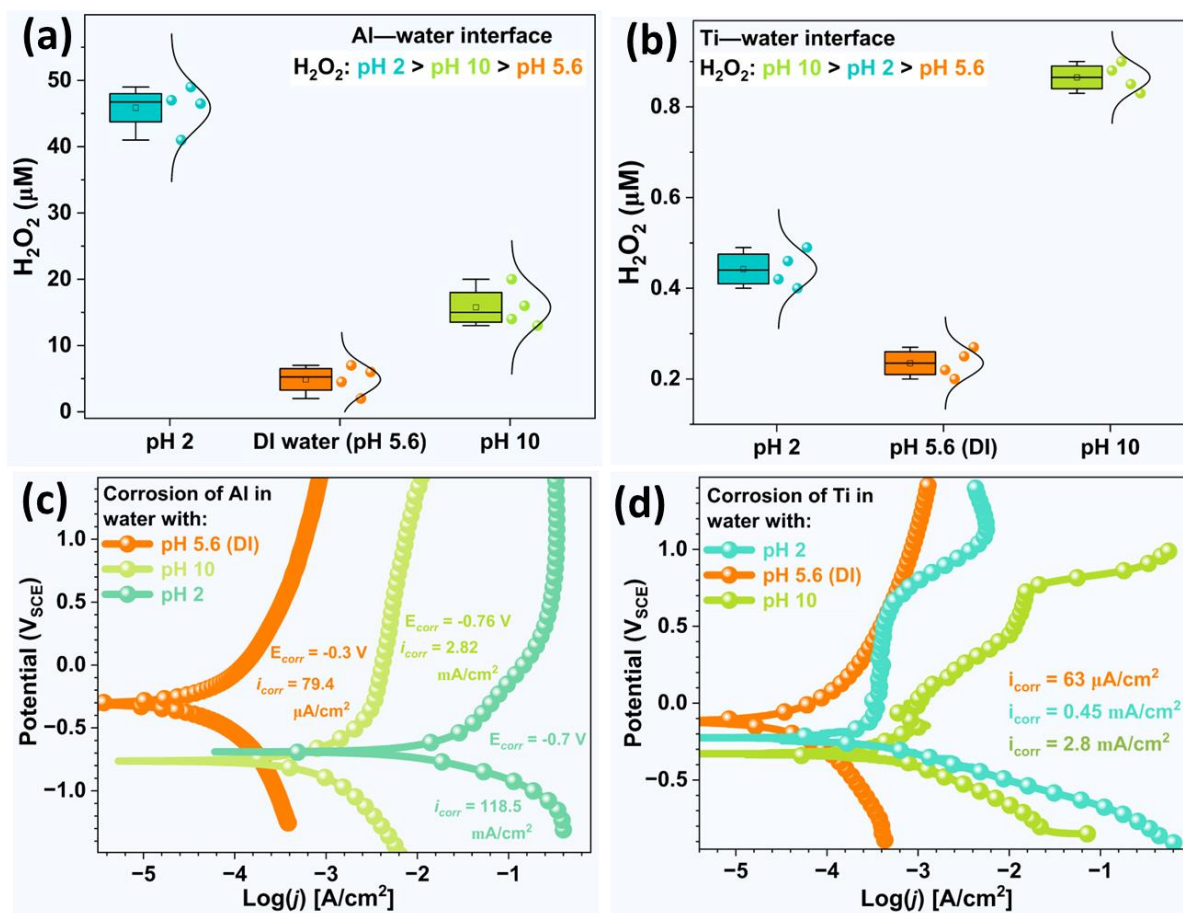


Figure 5 Effect of pH on H₂O₂ formation at water–solid interface. **(a)** Effect of pH on the H₂O₂ produced at the Al–water interface. **(b)** Effect of pH on the H₂O₂ produced at the Ti–water interface. **(c)** Effect of pH on the oxidation or corrosion behavior of the Al–water interface. **(d)** Effect of pH on the oxidation or corrosion behavior of the Ti–water interface.

In summary, our experimental results on the effect of halide anions or solution pH on H₂O₂ formation revealed that H₂O₂ is directly related to the oxidation of solid material at the solid–water interface. The solution conditions that lead to more corrosion of the solid surface led to more H₂O₂ formation. While we explore the oxidation of two metallic materials (Al & Ti) in this paper, other non-metallic materials (like glass) also get corroded in aqueous solutions and produce H₂O₂.^{14, 38, 39}

Conclusion

Taken together, our experimental results demonstrate that the air–water interface or the microdroplet geometry is incapable of spontaneously forming H₂O₂ regardless of the halides or the presence/absence of O₂. We have pinpointed solid–water interfaces as the sites for the

spontaneous H₂O₂ formation – only in the presence of O₂, i.e., no O₂, no H₂O₂. In this process, O₂ is reduced, and the solid surface is oxidized (i.e., corrosion). While solid–water interfaces can be conveniently bypassed in computer simulations, it is not possible inside a physical laboratory. Thus, we refute the previously reported mechanisms and conclusions, identifying the air–water interface as the site for spontaneous H₂O₂ formation^{1, 2, 4, 8, 10-12, 29-31}.

Methods:

Chemicals.

The following chemicals were purchased from Sigma Aldrich: sodium chloride (NaCl, 7647145), sodium bromide (CAS #7758-02-3), standard hydrogen peroxide (H₂O₂) 30% (Cat.270733), HPLC grade water (Cat. 2594649). Sodium iodide was obtained from Ward's Science (CAS #7681825). Water was obtained from a MilliQ Advantage 10 set up (with resistivity 18.2 MΩ cm) and referred to as “deionized” (DI). The HPAK (fluorometric-near infrared) kit was purchased from Abcam[®] (ab138886).

Quantification of H₂O₂

The concentration of H₂O₂ in all the diluted salt solutions was determined utilizing the hydrogen peroxide assay kit (HPAK) and cross-validated by NMR (described below). The HPAK method relies on the interaction between hydrogen peroxide and the AbIR peroxidase indicator, leading to fluorescence emission. The maximum excitation and emission wavelengths for this reaction are 647 nm and 674 nm, respectively. To analyze the samples, a mixture of 50 μL of HPAK reaction solution and 50 μL of the samples was prepared in a 96-well black/transparent bottom microtiter plate and read using a SpectraMax M3 microplate reader. The fluorescence data were processed using the SoftMax Pro 7 software. The H₂O₂ content in the samples was quantified by referencing the calibration curve established with standard samples on the same day.

NMR spectroscopy for H₂O₂(aq) quantification

Nuclear Magnetic Resonance (NMR) measurements were carried out utilizing the 950 MHz Bruker Avance Neo NMR spectrometer, which was equipped with a 5-mm Z-axis gradient TXO Cryoprobe and operated at 275 K. In all experiments, a 6-ms Gaussian 90-degree pulse

was utilized to excite the proton of hydrogen peroxide, followed by a 50-ms data acquisition period and a 1-ms recycling delay. The quantification of peak intensities and the verification of peak positions corresponding to H₂O₂ in salt solutions were conducted by comparing the results obtained from standard H₂O₂ samples. A total of 50000 scans were recorded in each case, which enables a detection of H₂O₂ as low as 50 nM.

Electrochemical testing

The corrosion behavior of solid specimens (Al, Ti) in aqueous solutions was assessed through potentiodynamic polarization tests. Right before each experiment, the specimens were meticulously polished using SiC grit papers up to 1200 grit, followed by cleansing with high-pressure N₂ gas. All experiments were conducted on specimens with a surface area of 1 cm², utilizing a BioLogic VMP3 potentiostat. A three-electrode system was consistently employed, with a platinum sheet (1 cm²) serving as the counter electrode and a saturated calomel electrode (SCE) as the reference electrode. The tests were carried out at a scan rate of 0.5 mV s⁻¹ and were performed. The open circuit potential (OCP) was only monitored for 5 seconds in each instance to prevent or minimize corrosion during the stabilization phase. The potentiodynamic polarization tests commenced at -500 mV with respect to the OCP.

Acknowledgments

The co-authors thank Dr. Adair Gallo and Ms. Nayara Musskopf for building a robust experimental setup in HM's laboratory; Dr. Ana Teresa Bigio, Scientific Illustrator, for the graphical abstract (TOC), Figure 1a, and Figure S1; Dr. Ryo Mizuta, Scientific Illustrator, for preparing illustrations Fig. 2b; Dr. Sankara Arunachalam and Dr. Krishna Katuri for helping with SEM imaging and providing a potentiostat for electrochemical measurements, respectively; Prof. Willem Koppenol (ETH Zurich) for fruitful discussions.

Author contributions: ME designed and performed the experiments and analyzed the data. HM oversaw the research and secured funding. ME and HM wrote the manuscript.

Competing interests: The authors declare no competing interests.

Data and materials availability: All data needed to evaluate the conclusions in the paper are present in the paper or the Supplementary Materials.

Funding: HM acknowledges KAUST for funding (Grant No. BAS/1/1070-01-01).

References

- (1) Lee, J. K.; Walker, K. L.; Han, H. S.; Kang, J.; Prinz, F. B.; Waymouth, R. M.; Nam, H. G.; Zare, R. N. Spontaneous generation of hydrogen peroxide from aqueous microdroplets. *Proceedings of the National Academy of Sciences of the United States of America* **2019**, *116* (39), 19294-19298.
- (2) Lee, J. K.; Han, H. S.; Chaikasetsin, S.; Marron, D. P.; Waymouth, R. M.; Prinz, F. B.; Zare, R. N. Condensing water vapor to droplets generates hydrogen peroxide. *Proceedings of the National Academy of Sciences of the United States of America* **2020**, *117* (49), 30934-30941.
- (3) Dulay, M. T.; Huerta-Aguilar, C. A.; Chamberlayne, C. F.; Zare, R. N.; Davidse, A.; Vukovic, S. Effect of relative humidity on hydrogen peroxide production in water droplets. *QRB Discovery* **2021**, *2*, e8. DOI: 10.1017/qrd.2021.6 From Cambridge University Press Cambridge Core.
- (4) Mehrgardi, M. A.; Mofidfar, M.; Zare, R. N. Sprayed Water Microdroplets Are Able to Generate Hydrogen Peroxide Spontaneously. *Journal of the American Chemical Society* **2022**, *144* (17), 7606-7609.
- (5) Peplow, M. Claims of water turning into hydrogen peroxide spark debate. In *C&EN*, American Chemical Society: 2022.
- (6) Kathmann, S. M.; Kuo, I. F. W.; Mundy, C. J.; Schenter, G. K. Understanding the Surface Potential of Water. *Journal of Physical Chemistry B* **2011**, *115* (15), 4369-4377.
- (7) Ben-Amotz, D. Electric buzz in a glass of pure water. *Science* **2022**, *376* (6595), 800-801.
- (8) Heindel, J. P.; Hao, H.; LaCour, R. A.; Head-Gordon, T. Spontaneous formation of hydrogen peroxide in water microdroplets. *The Journal of Physical Chemistry Letters* **2022**, *13* (43), 10035-10041.
- (9) Xiong, H.; Lee, J. K.; Zare, R. N.; Min, W. Strong Electric Field Observed at the Interface of Aqueous Microdroplets. *The Journal of Physical Chemistry Letters* **2020**, *11* (17), 7423-7428.
- (10) Colussi, A. J. Mechanism of Hydrogen Peroxide Formation on Sprayed Water Microdroplets. *Journal of the American Chemical Society* **2023**, *145* (30), 16315-16317.
- (11) Colussi, A. J. Physical Chemistry of Water Microdroplets. *The Journal of Physical Chemistry Letters* **2025**, *16* (13), 3366-3370.
- (12) Qiu, L.; Cooks, R. G. Spontaneous Oxidation in Aqueous Microdroplets: Water Radical Cation as Primary Oxidizing Agent. *Angewandte Chemie International Edition* **2024**, *63* (17), e202400118.
- (13) Eatoo, M. A.; Wehbe, N.; Kharbatia, N.; Guo, X.; Mishra, H. Why do some metal ions spontaneously form nanoparticles in water microdroplets? Disentangling the contributions of the air-water interface and bulk redox chemistry. *Chem Sci* **2025**, *16* (3), 1115-1125. DOI: 10.1039/d4sc03217a
- (14) Eatoo, M. A.; Mishra, H. Busting the myth of spontaneous formation of H₂O₂ at the air-water interface: contributions of the liquid-solid interface and dissolved oxygen exposed. *Chem Sci* **2024**, *15* (9), 3093-3103. DOI: 10.1039/d3sc06534k

- (15) Gallo Jr, A.; Musskopf, N. H.; Liu, X.; Yang, Z.; Petry, J.; Zhang, P.; Thoroddsen, S.; Im, H.; Mishra, H. On the formation of hydrogen peroxide in water microdroplets. *Chemical Science* **2022**, *13* (9), 2574-2583.
- (16) Musskopf, N. H.; Gallo, A.; Zhang, P.; Petry, J.; Mishra, H. The Air–Water Interface of Water Microdroplets Formed by Ultrasonication or Condensation Does Not Produce H₂O₂. *The Journal of Physical Chemistry Letters* **2021**, *12* (46), 11422-11429.
- (17) Koppenol, W. H.; Sies, H. Was hydrogen peroxide present before the arrival of oxygenic photosynthesis? The important role of iron(II) in the Archean ocean. *Redox Biology* **2024**, *69*, 103012.
- (18) Martins-Costa, M. T.; Ruiz-López, M. F. Probing solvation electrostatics at the air–water interface. *Theoretical Chemistry Accounts* **2023**, *142* (3), 29.
- (19) Gong, K.; Nandy, A.; Song, Z.; Li, Q.-S.; Hassanali, A.; Cassone, G.; Banerjee, S.; Xie, J. Revisiting the Enhanced Chemical Reactivity in Water Microdroplets: The Case of a Diels–Alder Reaction. *Journal of the American Chemical Society* **2024**.
- (20) Chen, C. J.; Williams, E. Are Hydroxyl Radicals Spontaneously Generated in Unactivated Water Droplets? *Angewandte Chemie International Edition* **2024**, e202407433. DOI: <https://doi.org/10.1002/anie.202407433> .
- (21) Chen, C. J.; Williams, E. R. A Source of the Mysterious m/z 36 Ions Identified: Implications for the Stability of Water and Unusual Chemistry in Microdroplets. *ACS Central Science* **2025**. DOI: 10.1021/acscentsci.5c00306.
- (22) Asserghine, A.; Baby, A.; N’Diaye, J.; Romo, A. I. B.; Das, S.; Litts, C. A.; Jain, P. K.; Rodríguez-López, J. Dissolved Oxygen Redox as the Source of Hydrogen Peroxide and Hydroxyl Radical in Sonicated Emulsive Water Microdroplets. *Journal of the American Chemical Society* **2025**, *147* (14), 11851-11858.
- (23) Trager, R. Water surprise: microdroplets have potential to produce hydrogen peroxide. In *Chemistry World*, Royal Society of Chemistry: 2019.
- (24) Cozens, T. Study casts doubt on water microdroplets’ ability to spontaneously produce hydrogen peroxide. In *Chemistry World*, Royal Society of Chemistry: 2022.
- (25) Nguyen, D.; Lyu, P.; Nguyen, S. C. Experimental and Thermodynamic Viewpoints on Claims of a Spontaneous H₂O₂ Formation at the Air–Water Interface. *The Journal of Physical Chemistry B* **2023**, *127* (11), 2323-2330.
- (26) Nguyen, D.; Nguyen, S. C. Revisiting the Effect of the Air–Water Interface of Ultrasonically Atomized Water Microdroplets on H₂O₂ Formation. *The Journal of Physical Chemistry B* **2022**, *126* (16), 3180-3185.
- (27) Trager, R. Water microdroplet chemistry is contentious, here’s why (<https://www.chemistryworld.com/news/water-microdroplet-chemistry-is-contentious-heres-why/4018721.article>). In *Chemistry World*, Royal Society of Chemistry: 2024.
- (28) LaCour, R. A.; Heindel, J. P.; Zhao, R.; Head-Gordon, T. The Role of Interfaces and Charge for Chemical Reactivity in Microdroplets. *J Am Chem Soc* **2025**, *147* (8), 6299-6317.
- (29) Li, K.; Guo, Y.; Nizkorodov, Sergey A.; Rudich, Y.; Angelaki, M.; Wang, X.; An, T.; Perrier, S.; George, C. Spontaneous dark formation of OH radicals at the interface of aqueous atmospheric droplets. *Proceedings of the National Academy of Sciences* **2023**, *120* (15), e2220228120.

- (30) Angelaki, M.; Carreira Mendes Da Silva, Y.; Perrier, S.; George, C. Quantification and Mechanistic Investigation of the Spontaneous H₂O₂ Generation at the Interfaces of Salt-Containing Aqueous Droplets. *J Am Chem Soc* **2024**, *146* (12), 8327-8334.
- (31) Angelaki, M.; d'Erceville, J.; Donaldson, D. J.; George, C. pH Affects the Spontaneous Formation of H₂O₂ at the Air-Water Interfaces. *J Am Chem Soc* **2024**, *146* (38), 25889-25893.
- (32) Chen, B.; Xia, Y.; He, R.; Sang, H.; Zhang, W.; Li, J.; Chen, L.; Wang, P.; Guo, S.; Yin, Y.; et al. Water–solid contact electrification causes hydrogen peroxide production from hydroxyl radical recombination in sprayed microdroplets. *Proceedings of the National Academy of Sciences* **2022**, *119* (32), e2209056119.
- (33) Benjamin, M. M. *Water Chemistry*; Waveland Press, Inc., 2015.
- (34) Kakeshpour, T.; Bax, A. NMR characterization of H₂O₂ hydrogen exchange. *Journal of Magnetic Resonance* **2021**, *333*, 107092. DOI: <https://doi.org/10.1016/j.jmr.2021.107092>.
- (35) Frankel, G. S. Pitting corrosion of metals - A review of the critical factors. *Journal of the Electrochemical Society* **1998**, *145* (6), 2186-2198.
- (36) Fontana, M. G. *Corrosion Engineering*; McGraw-Hill Book Company, 1985.
- (37) Ahmad, Z. *Principles of Corrosion Engineering and Corrosion Control*; Butterworth-Heinemann, 2006. DOI: <https://doi.org/10.1016/B978-0-7506-5924-6.X5000-4>.
- (38) Frankel, G. S.; Vienna, J. D.; Lian, J.; Scully, J. R.; Gin, S.; Ryan, J. V.; Wang, J. W.; Kim, S. H.; Windl, W.; Du, J. C. A comparative review of the aqueous corrosion of glasses, crystalline ceramics, and metals. *Npj Materials Degradation* **2018**, *2* (1).
- (39) Gin, S.; Dillmann, P.; Birbilis, N. Material degradation foreseen in the very long term: the case of glasses and ferrous metals. *Npj Materials Degradation* **2017**, *1* (1).

Supplementary Information

Disentangling the Roles of Dissolved Oxygen, Common Salts, and pH on the Spontaneous Hydrogen Peroxide Production in Water: No O₂, No H₂O₂

Muzzamil Ahmad Eatoo^{1,2,*} & Himanshu Mishra^{1,2,*}

¹ Environmental Science and Engineering (EnSE) Program, Biological and Environmental Science and Engineering (BESE) Division, King Abdullah University of Science and Technology (KAUST), Thuwal, 23955-6900, Kingdom of Saudi Arabia

² Interfacial Lab (iLab), King Abdullah University of Science and Technology (KAUST), Thuwal 23955-6900, Saudi Arabia

*Correspondence: muzzamil.eatoo@kaust.edu.sa and himanshu.mishra@kaust.edu.sa

Section S1. Spray setup for microdroplet formation

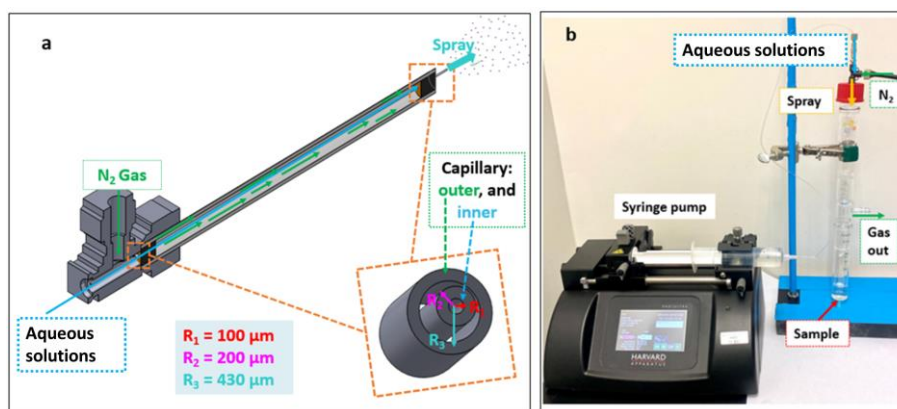


Fig. S1: (a) Schematics of pneumatic spray setup. (b) Photograph of a spray setup featuring a detachable glass flask for sample collection, incorporating two coaxial capillary tubes. The liquid sample is delivered through the inner capillary, while nitrogen gas flows through the surrounding outer annulus. Halide salt solutions were introduced using a syringe pump, and nitrogen gas was supplied from a high-pressure cylinder. The resulting microdroplets were sprayed and collected in a clean glass flask until an adequate volume of analyte had been obtained.^{1,2}

Section S2. Chemicals and Experimental Methods

S2.1 Chemicals: The following chemicals were purchased from Sigma Aldrich: sodium chloride (NaCl, 7647145), sodium bromide (CAS #7758-02-3), standard hydrogen peroxide (H₂O₂) 30% (Cat.270733), HPLC grade water (Cat. 2594649). Sodium iodide was obtained from Ward's Science (CAS #7681825). Water was obtained from a MilliQ Advantage 10 set up (with resistivity 18.2 MΩ cm) and referred to as “deionized” (DI). The HPAK (fluorometric-near infrared) kit was purchased from Abcam[®] (ab138886).

S2.2 Measurement of H₂O₂ formation in microdroplets: The microdroplets were formed by spraying bulk solutions at a flow rate of 25 μL/min using high-pressure (100 psi) dry N₂ gas. After spraying, the microdroplets were collected, and H₂O₂ was measured using ¹H-NMR. Nuclear Magnetic Resonance (NMR) measurements were carried out utilizing the 950 MHz Bruker Avance Neo NMR spectrometer, which was equipped with a 5-mm Z-axis gradient TXO Cryoprobe and operated at 275 K. In all experiments, a 6-ms Gaussian 90-degree pulse was utilized to excite the proton of hydrogen peroxide, followed by a 50-ms data acquisition period and a 1-ms recycling delay. Over 50000 scans were collected with a recycle delay of 1 ms between scans¹.

S2.3 Examination of H₂O₂ formation in bulk solution. The H₂O₂ formation at the solid-water interface in bulk solutions was examined using Metal samples (Al or Ti). Metal specimens of the same total surface area were submerged in different solutions of equal volumes, and the H₂O₂ formed was measured using ¹H-NMR and HPAK methods.

S2.4 Investigation of the oxidation rate of the solid surface.

The corrosion behavior of solid specimens (Al, Ti) in aqueous solutions was assessed through potentiodynamic polarization tests. Right before each experiment, the specimens were meticulously polished using SiC grit papers up to 1200 grit, followed by cleansing with high-pressure N₂ gas. All experiments were conducted on specimens with a surface area of 1 cm², utilizing a BioLogic VMP3 potentiostat. A three-electrode system was consistently employed, with a platinum sheet (1 cm²) serving as the counter electrode and a saturated calomel electrode (SCE) as the reference electrode. The tests were carried out at a scan rate of 0.5 mV s⁻¹ and were performed. The open circuit potential (OCP) was only monitored for 5 seconds in each instance to prevent or minimize corrosion during the stabilization phase. The potentiodynamic polarization tests commenced at -500 mV with respect to the OCP.³

S2.5. Quantification of H₂O₂ in sprayed water microdroplets by HPAK kit.

The concentration of H₂O₂ in all the diluted salt solutions was determined utilizing the hydrogen peroxide assay kit (HPAK). This method relies on the interaction between hydrogen peroxide and the AbIR peroxidase indicator, leading to fluorescence emission. The maximum excitation and emission wavelengths for this reaction are 647 nm and 674 nm, respectively. To analyze the samples, a mixture of 50 μL of HPAK reaction solution and 50 μL of the samples was prepared in a 96-well black/transparent bottom microtiter plate and read using a SpectraMax M3 microplate reader. The fluorescence data were processed using the SoftMax Pro 7 software. The H₂O₂ content in the samples was quantified by referencing the calibration curve established with standard samples on the same day

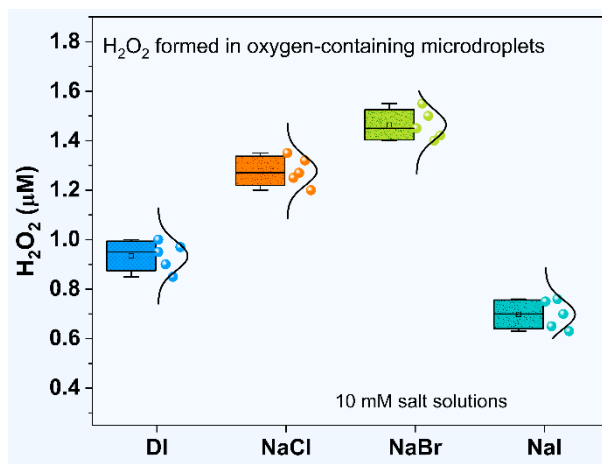


Figure S2. Quantification of H₂O₂ formed in sprayed microdroplets by HPAK.

Section S3. Oxidation of iodide ions to triiodide by H₂O₂

Oxidation of iodide ions to triiodide due to H₂O₂ produced by the Al specimen in 10 mM NaI solution in 1 day. The oxidation of iodide ions by H₂O₂ produced at the Al-water interface due to O₂ reduction, to triiodide, was examined by UV-vis spectroscopy. Blank 10mM NaI without metal specimen was used as a reference sample. And the 10 mM NaI sample with a freshly polished Al specimen for 24 hours was scanned in the range of 200-600 nm using quartz cuvettes with a 1 cm path length. The triiodide ion (I₃⁻) typically shows a characteristic absorption peak near 350 nm, and a weaker band around 290 nm was observed, as shown in Figure S4 below.

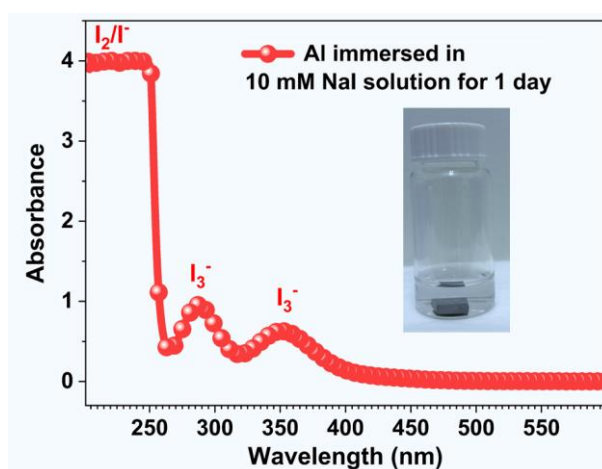


Fig. S3. shows the formation of triiodide in NaI solution due to the presence of H₂O₂ formed by the Al sample in the 10 mM solution.

Section S4. Pitting corrosion by Cl^- ions

We investigated the Al surfaces after exposure to salty solutions via scanning electron microscopy (SEM) (Fig. S5) and found and paid closer attention to the polarization curves given in Fig. 4a. It is evident from both polarization curves and micrographic images that the Al surface undergoes severe pitting attack at higher NaCl concentrations. In Fig. 4a, the pitting is represented by a sudden increase in anodic currents. It can be clearly observed that 10 mM and 50 mM salt concentrations cause severe pitting. The pits formed in the solid Al surface can also be clearly seen in SEM micrographs (Fig. S5).

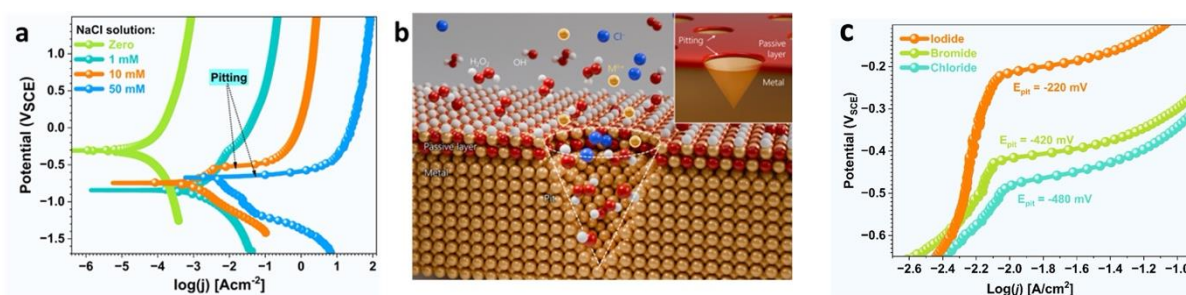


Fig. S4 The effect of Cl^- concentration on corrosion behavior of Al (AA5083) in NaCl solutions. **a)** Potentiodynamic polarization curves showing pitting of Al in 10 mM and 50 mM NaCl solutions. **b)** Illustration showing the pitting or passive layer breakdown phenomenon by Cl^- ions. **(c)** The effectiveness of Cl^- , Br^- , and I^- ions to cause pitting. The data shows the pitting potentials of Al in 10 mM solutions of NaCl, NaBr, and NaI.

The pitting tendency of different halide anions was also examined by measuring the pitting potentials. The pitting potentials of Al in 10 mM salt solutions of NaCl, NaBr, and NaI are around -480, -420, and -220 mV, respectively (Fig. S4-c). This shows that among different halide anions, chloride has the highest pitting power. Therefore, the pitting power of halide ions follows the trend $\text{Cl}^- > \text{Br}^- > \text{I}^-$.

Section S5. SEM imaging of Al after exposure to NaCl solution.

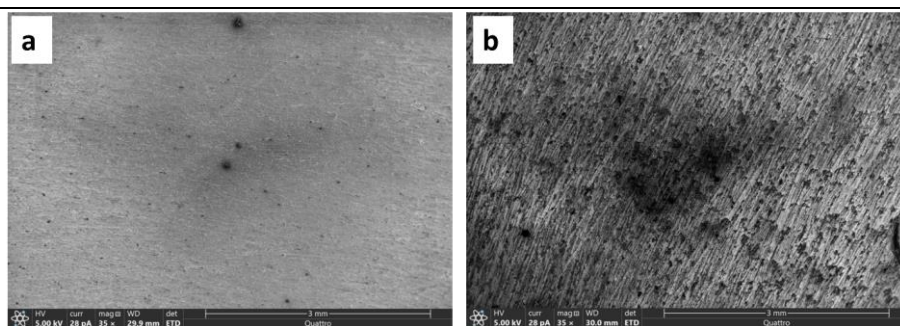


Fig. S5. SEM images of Al immersed for 24 hours in: a) 10 mM NaCl solution. b) 50 mM NaCl solution. The pitting attack represented by pore-like features in the images can be clearly observed. Also, in 50 mM NaCl solution, the high pit density and damage of the oxide layer on the surface are evident. This pitting or film breakdown brings the naked metal surface in direct contact with H_2O_2 present in the solution. After that, the H_2O_2 gets consumed by the metal surface.

Section S6: To examine the effect of pitting or passive film breakdown on H_2O_2 present in the solution, we investigated the interaction of H_2O_2 with the fresh metal surface (polished) and thermally grown oxide on the metal/Al surface. We prepared a $100 \mu\text{M}$ H_2O_2 solution using deaerated water so that the Al samples do not produce any H_2O_2 . We immersed Al samples having the same surface area (2.3 cm^2) in equal volumes of $100 \mu\text{M}$ H_2O_2 solutions. One of the samples was freshly polished to remove any impurity or oxide on its surface, and an oxide layer was thermally grown on the other sample by heating it at $\sim 500 \text{ }^\circ\text{C}$ in a muffle furnace for 12 hours in the presence of O_2 . The results obtained after 1 hour of immersion in H_2O_2 solution are shown in Fig. S6. The results revealed that H_2O_2 is consumed more by the fresh metal surface as compared to one covered with an oxide layer.

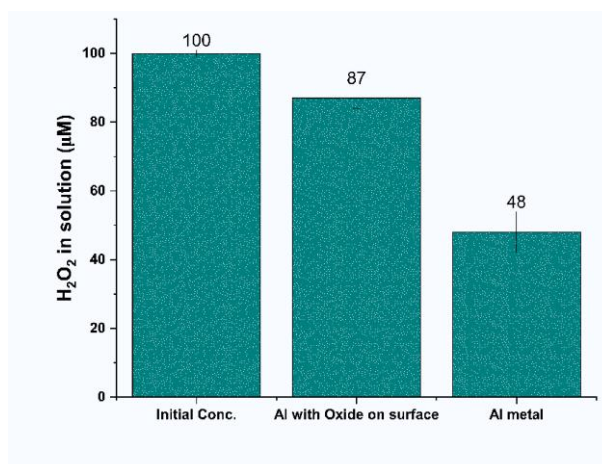


Fig. S6 Comparison of H_2O_2 consumption by fresh metal surface vs the surface with oxide layer.

References:

- (1) Eatoo, M. A.; Mishra, H. Busting the myth of spontaneous formation of H₂O₂ at the air-water interface: contributions of the liquid-solid interface and dissolved oxygen exposed. *Chem Sci* **2024**, *15* (9), 3093-3103.
- (2) Eatoo, M. A.; Wehbe, N.; Kharbatia, N.; Guo, X.; Mishra, H. Why do some metal ions spontaneously form nanoparticles in water microdroplets? Disentangling the contributions of the air-water interface and bulk redox chemistry. *Chem Sci* **2025**, *16* (3), 1115-1125.
- (3) Raja, V. S.; Eatoo, M. A.; Agrawal, R. K.; Palli, S.; Krishnan, M. A. Role of Strontium on Sensitization and Unusual Passivation Behavior of a 5xxx Series Aluminum Alloy Containing a Trace Amount of Chromium. *Journal of the Electrochemical Society* **2023**, *170* (3). DOI: ARTN 03150710.1149/1945-7111/acc489